

Unveiling hidden charge density waves in single-layer NbSe₂ by impurities

Fabrizio Cossu^{1,*}, Ali G. Moghaddam^{2,†}, Kyoo Kim³, Hassan A. Tahini^{4,5},

Igor Di Marco^{1,6}, Han-Woong Yeom^{7,8}, and Alireza Akbari^{1,3,7,‡}

¹*Asia Pacific Center for Theoretical Physics, Pohang, Gyeongbuk 790-784, Korea*

²*Department of Physics, Institute for Advanced Studies in Basic Sciences (IASBS), Zanjan 45137-66731, Iran*

³*Max Planck POSTECH Center for Complex Phase Materials, POSTECH, Pohang 790-784, Korea*

⁴*Department of Applied Mathematics, Research School of Physics and Engineering,
Australian National University, Canberra 0200, Australia*

⁵*Integrated Materials Design Centre (IMDC), School of Chemical Engineering, UNSW Australia, Sydney, NSW 2052, Australia*

⁶*Department of Physics and Astronomy, Uppsala University, Box 516, SE-75120, Uppsala, Sweden*

⁷*Department of Physics, POSTECH, Pohang, Gyeongbuk 790-784, Korea and*

⁸*Institute for Basic Science Korea, Center for Artificial Low Dimensional Electronic Systems Pohang 790784, South Korea*
(Dated: December 3, 2022)

We employ *ab-initio* calculations to investigate the charge density waves in NbSe₂ single layers, and we explore how they are affected by transition metal atoms. Our calculations reproduce the observed orthorhombic phase in NbSe₂ single layer in the clean limit, establishing the energy order between three different distorted structures, two consisting of triangular Nb-Nb clusters and a third, energetically unfavoured, consisting of hexagonal Nb-Nb clusters. Such energy order, in agreement with known experimental work, is reversed by the adsorption of Co and Mn, which favour the formation of hexagonal Nb-Nb clusters; this CDW structure is indeed allowed from symmetry point of view but hidden in pure single-layers because it is at a higher energy. The other adsorbates, K and Ga, still favour one of the triangular Nb-Nb cluster, while suppressing the other. We report how the energy difference between such distorted structure varies with these adsorbates. Furthermore, transition metals induce magnetism and favour the reduction of the symmetry of the charge density distribution.

I. INTRODUCTION

Over the past decade, synthesis and exploration of atomically thin two-dimensional (2D) materials have almost revolutionized our common understandings of condensed matter systems and opened a new era in nanosciences [1–3]. In particular, 2D materials usually show drastically different electronic properties compared to their corresponding bulk structures composed of van der Waals (vdW) coupled atomic layers [4–6]. Transition metal dichalcogenides (TMDCs) are among vdW layered materials which show a wide range of interesting phenomena and applications due to the tunability of their electronic structures [7–10]. Moreover, they can host exotic phases, such as superconductivity (SC), charge density waves (CDW), and even topologically non-trivial states [11–15]. Strongly correlated phases in bulk TMDCs have been well studied for decades, and recent observations of CDWs and the so-called Ising SC in the 2D single-layers have triggered renovated interest in them [16–20].

Among TMDCs, NbSe₂ has been considered as a prototype material for investigation of CDW orders and SC [21, 22]. Bulk 2H-NbSe₂ hosts a CDW phase with a 3×3 periodicity below 33K which can coexist with an s-wave superconducting phase below 7K [23–27], and it is known for its high magnetic anisotropy [28]. Intriguingly, by reducing its thickness down to single-layers, while the SC

weakens but still survives, the CDW transition temperature increases up to 145 K [12, 16, 18]. The coexistence of SC and CDW phases in NbSe₂ suggested that the electronic states involved in the CDW transition are primarily away from Fermi level which leaves a room for the establishment of superconducting correlation [19, 29]. The origin of the CDWs has been intensively debated for some TMDCs including NbSe₂ mostly because of controversies over the role of Fermi-surface nesting [30–37]. Nevertheless, in recent years theoretical and experimental evidences has been accumulated in support of momentum-dependent electron-phonon coupling as a key mechanism in the formation of CDWs [38–40]. Turning to 2D single-layers, the lack of inversion symmetry, the disappearance of the coterminous of vdW interactions and the interplay with many-body strong-correlation effects may lead to the aforementioned drastic changes [41–43].

On the other hand, the structure of CDWs in bulk and single-layer NbSe₂ has been controversial [44–46]. While a recent detailed experimental work has reported a 3×3 commensurate modulation of the crystal structure, the case of the single-layer still needs to be clarified [38, 45]. In addition, impurities or gate doping can play a major role on the CDW behaviour. For example, long-range CDW phase coherence can be suppressed by high percentage of Co or Mn intercalated in NbSe₂ surfaces [47] and hole doping [19], while it can be increased by electron doping [19]. Besides, Bi adsorption can also lead to a transition to a stripe phase [48], previously observed in accidentally doped samples [49].

In this work, performing an exhaustive first principle calculations, we reveal possible structures of CDWs, par-

* fabrizio.cossu@apctp.org

† agorbanz@iasbs.ac.ir

‡ alireza@apctp.org

ticularly at the presence of certain types of impurities. Among three different modulated structures, those two with triangular Nb-Nb clusters are found to be energetically favored in clean NbSe₂ 2D sheet. These results are consistent with experimental evidence [44, 45]. As a key finding we demonstrate that CDWs with hexagonal modulation can be established by adsorption of certain atoms such as Co and Mn. This type of CDW phase is in fact hidden in pristine NbSe₂ because it has a higher energy compared to triangularly-modulated CDWs. In addition, it is uncovered that the presence of the transition metal impurities induces magnetism and promotes modulated phases with reduced symmetry of the charge density distribution compared to pure CDW structures. Other types of metallic ad-atoms, namely K and Ga, allow the same ground state as pristine single-layer NbSe₂, but Ga also supports the hexagonally modulated structure. The current manuscript aims at steering future research towards a new interpretation of the experimental evidence on the effect of impurities [47–49], and represents an important contribution in the field of the interplay between CDWs and SC, as a recent work strongly points out [50].

This paper is organized as follows. In Sec. II, we will briefly introduce the computational method based on density functional theory which is used for investigation of CDW phases. Thereafter, we go through the results of *ab-initio* calculations for CDWs in pristine NbSe₂, Sec. III, where the relaxed CDW structures and the profiles of charge densities are presented both in real space and in Fourier transformed form. The core of our work is found in Sec. IV, which shows the CDWs in the presence of various impurities. In particular, we show how the energy hierarchy of the CDWs can be different from the pristine system and a hidden order arise as a new ground state by adding Co or Mn ad-atoms. Finally, after a discussion over the results, the conclusions are presented in Sec. V.

II. COMPUTATIONAL DETAILS

Our results are obtained by means of density-functional theory (DFT). We employ the projected augmented wave (PAW) method with Perdew-Burke-Ernzerhof (PBE) pseudopotentials, as implemented in the Vienna *ab initio* Simulation Package (VASP) [51, 52]. Accordingly, the exchange-correlation functional is treated in the generalised gradient approximation in the PBE parametrisation [53, 54]. The basis set consists of plane waves, with the explicit treatment of 13, 6, 9, 15, 9 and 13 valence electrons for Nb, Se, Co, Mn, K and Ga states, respectively. As previously suggested [55], standard local and semi-local exchange-correlation functionals may not offer a proper description of the partially filled 3*d* and 4*f* shells of TM adatoms on 2D materials. Therefore, calculations are performed in the DFT+U approach, using the rotationally invariant formulation of Lichtenstein *et al.* [56]. As in ref. [55], we used a gen-

eralized value of $U = 4.00$ eV and $J = 0.90$ eV for all Co and Mn. For all calculations, the cutoff energy of the plane waves is 400 eV, while the energy tolerance on the electronic loops for the relaxation and for the electronic properties are set to 10^{-6} eV and 10^{-7} eV, respectively; a conjugate gradient algorithm is employed for structural relaxation. Structures are considered relaxed when the forces on each atom are smaller than 2 meV/Å. The simulations are run in $3 \times 3 \times 1$, $6 \times 6 \times 1$ and $9 \times 9 \times 1$ replicas of the NbSe₂ single layer unit cell. After convergence tests on the \mathbf{k} -meshes for the $3 \times 3 \times 1$ and $6 \times 6 \times 1$ replicas were performed, $15 \times 15 \times 1$, $7 \times 7 \times 1$ and $5 \times 5 \times 1$ grids of \mathbf{k} -points were used to sample their Brillouin Zones for the total energy calculations; $11 \times 11 \times 1$ and $5 \times 5 \times 1$ \mathbf{k} -meshes were used for the partial charge density calculations in the $6 \times 6 \times 1$ and $9 \times 9 \times 1$ replicas, respectively; a $45 \times 45 \times 1$ \mathbf{k} -mesh was used for the DOS calculations in the $3 \times 3 \times 1$ replica. In modelling metal adsorption on NbSe₂, the concentration of one ad-atom in a $6 \times 6 \times 1$ replica of the unit cell was adopted, corresponding to 0.0278 impurities/f.u., which allows for a description of a $3 \times 3 \times 1$ CDW while minimising the interaction between impurities and their images. The adsorbates taken into account in the present study are Co, Mn, K and Ga.

III. CDW PHASES IN PRISTINE SINGLE-LAYERS

We begin with the study of the single layer NbSe₂ in a $3 \times 3 \times 1$ supercell, which is the minimal size cell for a CDW in NbSe₂. Pristine single layer NbSe₂ is known to be metallic, non magnetic and hosts CDWs below 145 K [13, 24, 57]. Our models include three structures obtained according to existing work [16, 44, 45], which are shown in Fig. 1; the Nb atoms cluster in triangular patterns - see Figs. 1(a and b) - and hexagonal ones - see Fig. 1(c); the two triangular patterns differ by the position of the Se atoms with respect to the triangle composed by the Nb-Nb bonds; accordingly, the CDW structures are named T-U, T-C and HX, respectively (T-U and T-C stand for triangle-uncentred and triangle-centred). The two structures T-U and T-C are related to each other by a mirror reflection of the Nb sublattice. It is also known that the Se-Se bond patterns (analogous to Nb-Nb bond patterns) accompany those of Nb-Nb [46]. The T-U and T-C CDWs differ for the Se-Se pattern, see the Appendix for details. Their total energies were compared in $3 \times 3 \times 1$ and $6 \times 6 \times 1$ replicas of the NbSe₂ unit cell, and suggest that the formation of all of them is favoured. The T-U is the lowest energy CDW structure; calculations in the $3 \times 3 \times 1$ supercell yield differences of 3.9 meV, 0.5 meV and 1.3 meV/f.u. with respect to the undistorted structure, T-C and HX, respectively. In the $6 \times 6 \times 1$ supercell, slight changes are observed in the energy differences between the CDW structures: the T-U is favoured by 0.4 meV and 1.1 meV over the T-C and HX, respectively; these differences are maintained for a $9 \times 9 \times 1$

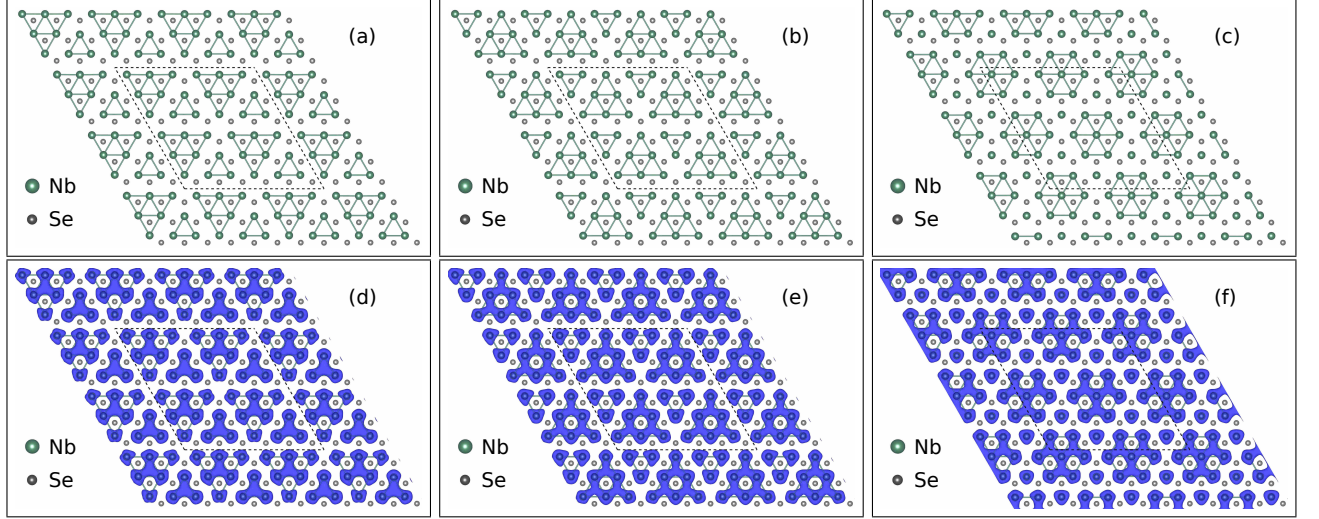


FIG. 1. (Colour online) First row: relaxed CDW structures for pristine NbSe₂ (top view): T-U (a), T-C (b) and HX (c) CDWs (see text for details); Second row: charge densities of the respective CDW structures. Volumetric data are represented as blue surfaces enclosing points whose electronic density is greater than or equal to 0.0075 electrons/Bohr³. Atoms are represented by spheres, as illustrated in the legends (magnified); Nb-Nb bonds shorter than the equilibrium distance (3.45 Å) are represented by solid lines, in order to help visualising the CDW structure pattern. Dashed lines mark the supercells borders.

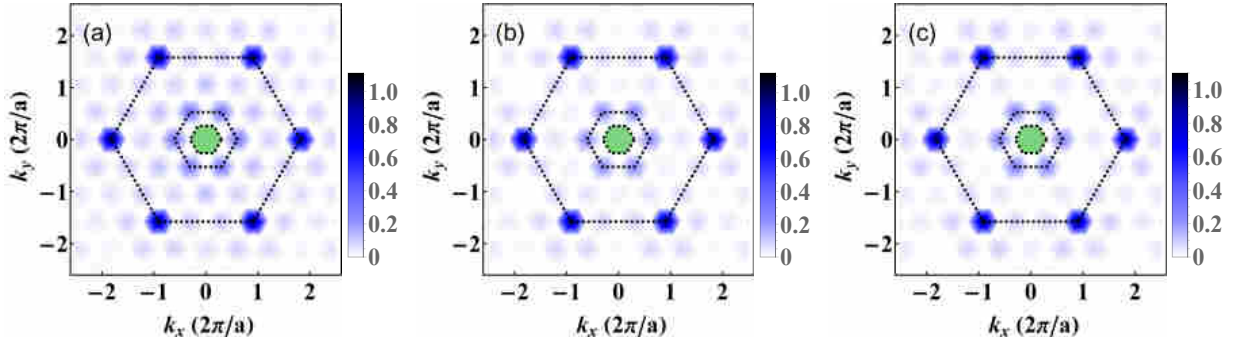


FIG. 2. (Colour online) Fourier Transform (FT) plots of the charge density distributions for the pristine T-U (a) T-C (b) and HX (c) structures, as given in Fig. 1. The large dashed hexagon with vertices at $|\mathbf{q}| = \frac{2\pi}{a}$ (with $a = 3.45$ Å) marks the characteristic Bragg peaks; the medium size dashed hexagon with vertices at $|\mathbf{q}| = \frac{2\pi}{3a}$ marks the (shorter) CDW peaks; the small green shaded hexagon ($|\mathbf{q}| = \frac{2\pi}{6a}$) maps points beyond the supercell borders,

supercell. The three CDW structures were recently investigated elsewhere on $3 \times 3 \times 1$ supercells [58]. Here, we demonstrate our agreement with ref. [58], and we make use of the results for the pristine to compare the metal-adsorbed NbSe₂.

The effect of the CDW distortions on the density of states (DOS) is analysed in the Appendix. For what concerns the electronic reconstruction following the CDW formation, our calculations are in agreement with the literature [38, 59]. The charge distributions are computed integrating the charge density over the occupied Nb band (the band crossing Fermi level, see the Appendix) and they are shown in Fig. 1, second row. The integration over the whole occupied band simulates a topography retaining the symmetry of the Nb band only. The charge density clusters in patches, with different shape and patterns for each CDW; the lowest energy CDWs, T-U and

T-C, have three-fold symmetric patterns and the HX CDW has six-fold symmetric ones. The patches of T-U are on the vertices of a hexagon (with no element on the centre), whereas those of T-C and HX are placed on the vertices and centre of a larger hexagon.

The Fourier Transform (FT) of the charge density distribution is crucial for the analysis of the CDW intensity - especially when comparing the pristine case with the doped case (see discussion in the next section). Due to the three-dimensional periodic boundary conditions, the three-dimensional data is originally computed as a function of the (h, k, l) Miller indices; the subset with $l = 0$ is analysed to track modulations of the CDW charge distributions only along the plane. Thus, the FT is mapped as a function of h and k (k_x and k_y in the relative plots). The computed FT of the charge densities in Fig. 2 show the characteristic Bragg peaks at the vertices

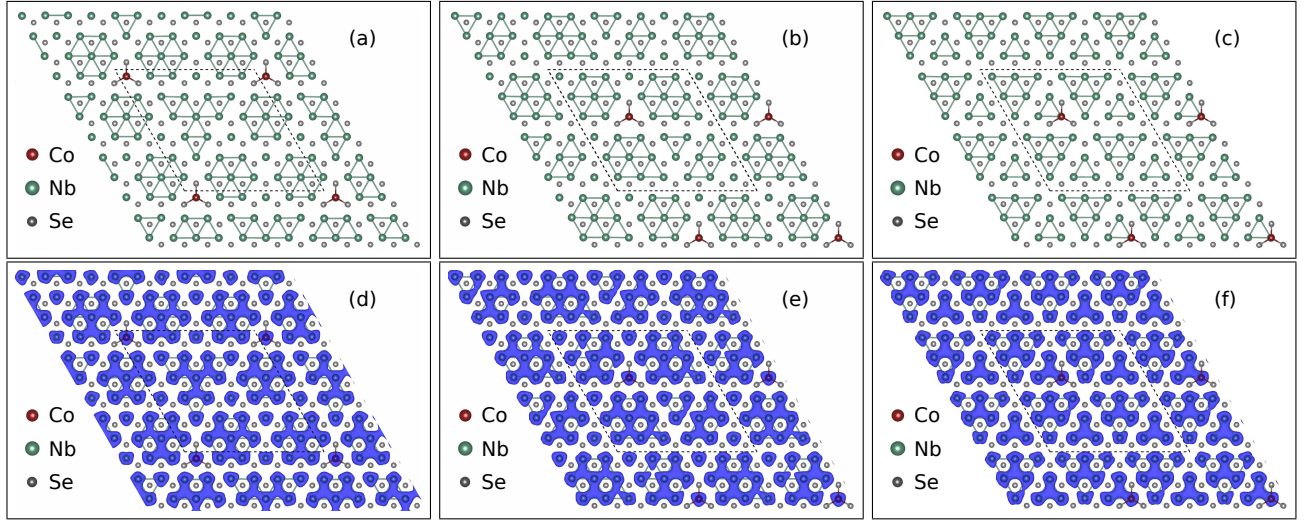


FIG. 3. (Colour online) First row: round state Co|NbSe₂ HX-S (a), HX-A (b) and T-U (c) CDW structure; Second row: charge densities of the respective CDW structures. The isosurface value for the volumetric data is set in agreement with Fig. 1. Atoms are represented by spheres, as illustrated in the legends; Nb-Nb bonds shorter than the equilibrium distance (3.45 Å) are represented by solid lines, to help visualising the CDW structure pattern. Dashed lines mark the supercells borders.

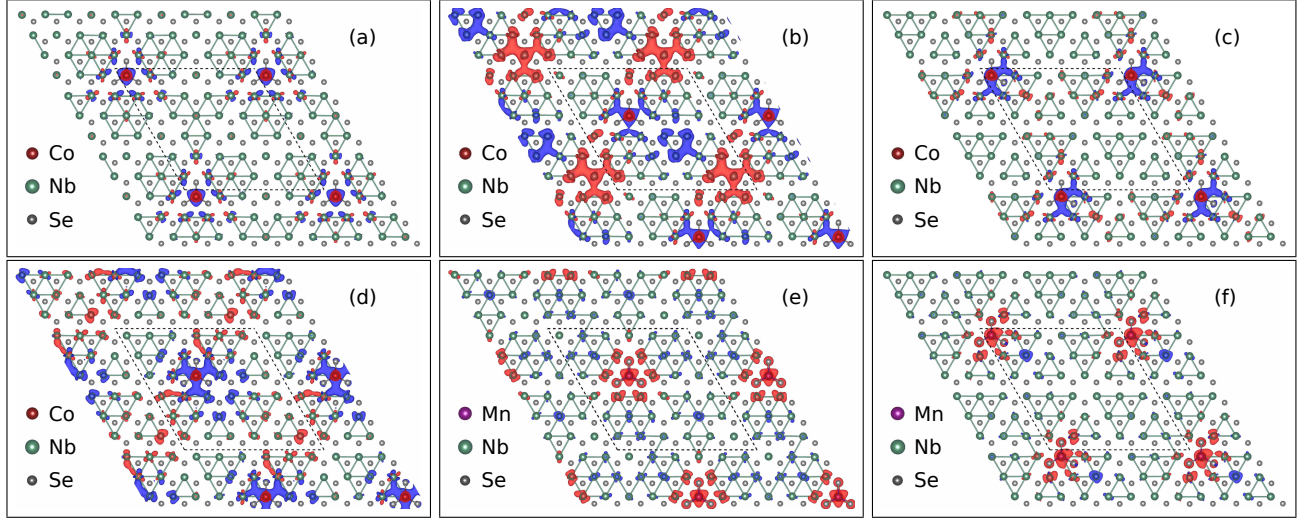


FIG. 4. (Colour online) Magnetisation densities of Co|NbSe₂ HX-S (a), Co|NbSe₂ HX-A (b), Co|NbSe₂ T-U at 1 (c), Co|NbSe₂ T-U at 3 (d), Mn|NbSe₂ HX-A (e) and Mn|NbSe₂ T-U at 1 (f). The magnetisation densities in (c) and (d) are different although they have virtually the same structure and total energy; the magnetisation in (c) is juxtaposed to (f) to compare structures with the same adsorption site. Volumetric data are represented as blue (red) surfaces enclosing points whose magnetisation density is greater than or equal to 0.0075 (smaller than or equal to -0.0075) μ_B/Bohr^3 . Atoms are represented by spheres, as illustrated in the legends; Nb-Nb bonds shorter than the equilibrium distance (3.45 Å) are represented by solid lines to help visualising the CDW structure pattern. Dashed lines mark the supercells borders.

of a hexagon, with vertices at $|\mathbf{q}| = \frac{2\pi}{a}$ (with $a = 3.45$ Å) and marked by dash lines, inside of which the shorter peaks of the CDW are found at the vertices of a medium size hexagon (with vertices at $|\mathbf{q}| = \frac{2\pi}{3a}$), also marked by dashed lines. The points inside the small green shaded hexagon ($|\mathbf{q}| = \frac{2\pi}{6a}$) map points beyond the supercell borders, and are therefore not meaningful. Due to the size of the supercell, the width of the spots denoting Bragg peaks or CDW peaks is large because different but close

modulation frequencies cannot be resolved, even with a relatively dense k-mesh.

IV. CDW PHASES IN THE PRESENCE OF IMPURITIES

Adsorption of the adsorbates Co, Mn, K and Ga on a fully symmetric structure induces structural distortions breaking the symmetry of the NbSe₂ layer according to

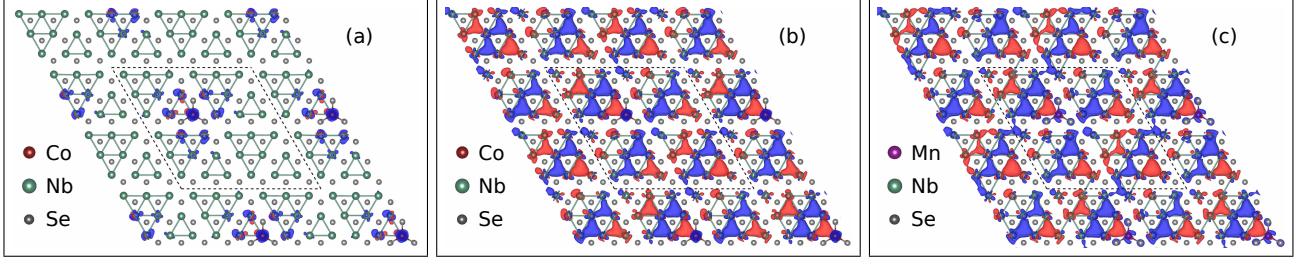


FIG. 5. (Colour online) Differences between charge density distributions. First row: Co|NbSe₂ T-U minus NbSe₂ T-U (a), Co|NbSe₂ HX-A minus NbSe₂ T-U (b) and Mn|NbSe₂ HX-A minus NbSe₂ HX (c). Volumetric data are represented as blue (red) surfaces enclosing points whose electronic density is greater than or equal to 0.0025 (smaller than or equal to -0.0025) electrons/Bohr³. Atoms are represented by spheres, as illustrated in the legends; Nb-Nb bonds shorter than the equilibrium distance (3.45 Å) are represented by solid lines to help visualising the CDW structure pattern. Dashed lines mark the supercells borders.

TABLE I. Energetics and magnetism for M|NbSe₂ (M = Co, K, Ga, Mn). Energies differences are computed with respect to the lowest configuration and are expressed in meV. Magnetic moments are expressed in μ_B .

		ΔE	μ^{TM}	μ_{tot}
Co	hollow	16	1.9	2.2
	top Nb	0	1.9	2.0
	top Se	3551	2.0	3.4
Mn	hollow	91	4.4	5.8
	top Nb	0	4.4	4.3
	top Se	1291	4.9	4.1
K	hollow	4	0.0	5.9
	top Nb	0	0.0	0.0
	top Se	241	0.0	1.2
Ga	hollow	183	0.0	5.9
	top Nb	0	0.0	0.0
	top Se	605	0.0	0.2

the site: the adsorption on the Nb site, hollow site and Se site induces CDWs of HX type (i.e. having similar Nb-Nb distance patterns), T-U type and T-C type, respectively. By total energy calculations, the likelihood of the adsorption sites is analysed. Along the lines of a study of the energetics of TM atoms on MoS₂ [60], we compared the energy at different adsorption sites for some ad-atoms, see TABLE I, obtaining a good agreement. The preferred adsorption site is on top of a Nb atom for Co, K, Ga and Mn. The competition between hollow site and Nb site is strong in the case of K (4 meV difference). The Se site remains the most unfavoured for single atoms. However, it competes with Nb for larger molecules. In order to highlight this trend, we computed the energy difference for Co-(OH)₂, which can be considered as a prototype of a small molecule and a possible impurity. In the case of a single Co, the Nb site is preferred to the hollow site and Se site by 16 meV and 3551 meV, respectively; in the case of Co-(OH)₂, the corresponding

TABLE II. Energetics for the CDWs in M|NbSe₂ (M = Co, Mn, K, Ga); the energy for each column (adsorbate) is given as differences with respect to the ground state. Different position and resulting structure are possible for each metal M adsorbed on a CDW; we report those which evolve to structures relatively close in energy to the ground state, mentioning the type of structure, when it is similar to one of the three pristine CDWs, as well as the energy difference. The difference in energy in the 9x9 supercell (1 Co) is 0.3 meV/f.u. in favour of the HX CDW.

pristine	Co	Mn	K	Ga
T-U (0.0)	T-U (0.7)	T-U (1.5)	T-Uh (0.0)	T-U (0.0)
	T-U (2.6)		T-UN (0.2)	
T-C (0.4)	HX-A (0.0)	HX-A (0.0)	T-CN (1.5)	HX-A (0.1)
			T-Ch (1.3)	
HX (1.1)	HX-S (0.0)	HX-S (0.0)	HX-S (0.7)	HX-S (0.0)
	HX-A (0.0)	HX-A (0.0)		

energy difference are ~ 670 meV and 166 meV, suggesting a hindrance to the Co-Se bonds and Co-Nb bonds or a decrease of the Co charge state and in turn of its coordination. In summary, single Co is preferably adsorbed on the Nb site, with the hollow site relatively close in energy; large molecules favour adsorption on the Se site and unfavour adsorption at the hollow site, a trend in line with combined theoretical and experimental results [61]. After establishing the preferred adsorption sites on the NbSe₂ non modulated structure for each adsorbate by total energy calculations, the adsorption on the different CDW structures is modelled (it involves different inequivalent adsorption sites due to the lower symmetry).

A. Adsorption of Co

Upon adsorption of Co, the energy and state of CDWs are modified. In general, the solutions are a combination of the states found in the pristine system. Pure solutions of the T-U CDW are found and are referred to as such in the remainder. The HX CDW solutions are found in mixed states or pure states; those with lowest energy are

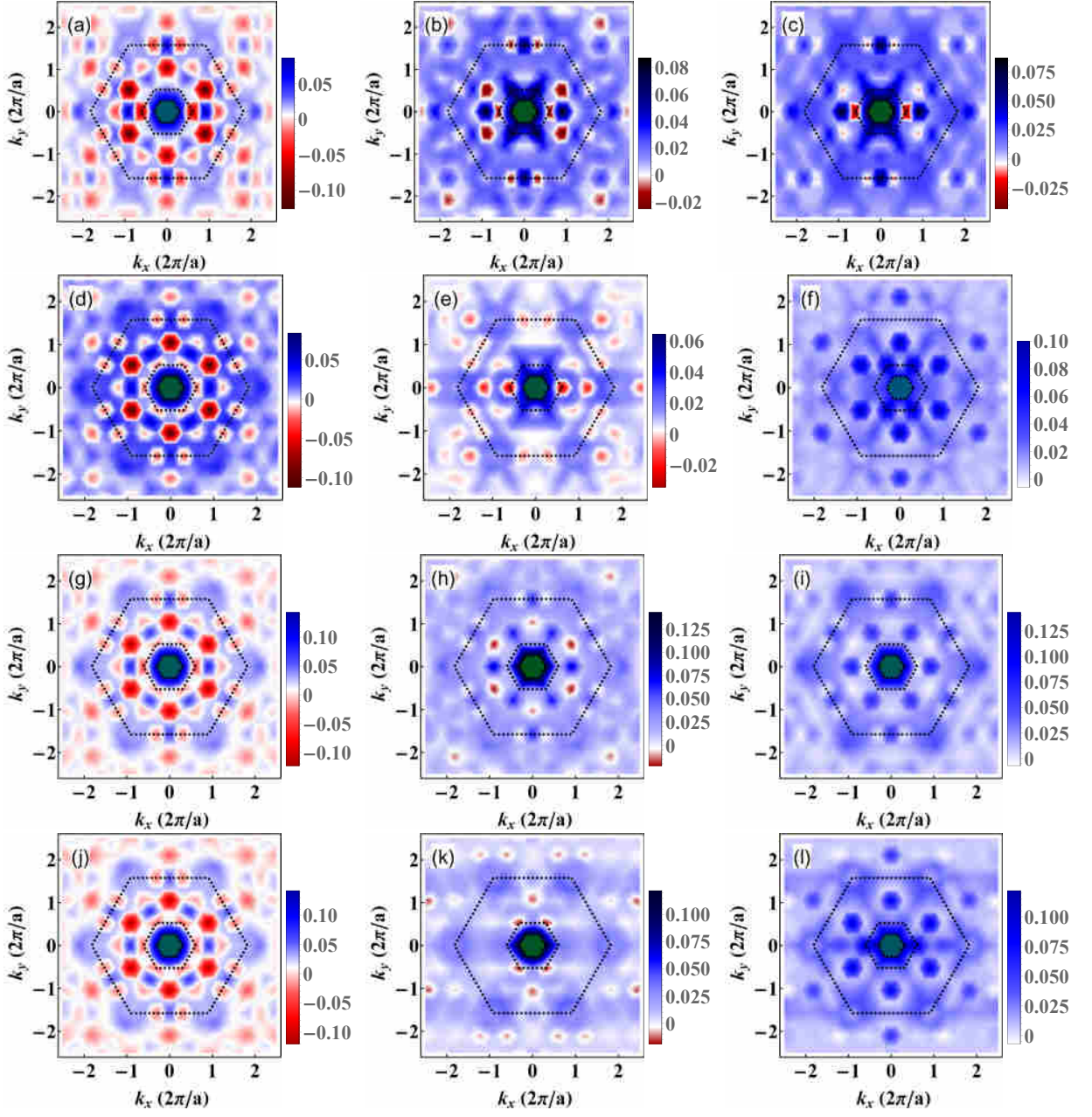


FIG. 6. (Colour online) Differences between FTs of the charge density distribution of Co|NbSe₂ CDWs and pristine NbSe₂. First row: ground state Co|NbSe₂ HX-A minus pristine T-U (a), T-C (b) and HX (c); Second row: ground state Co|NbSe₂ HX-S minus T-U (d), Co|NbSe₂ T-U minus pristine T-U (e) and Co|NbSe₂ T-U minus pristine T-C (f). The third and the fourth line are analogous to the first and the second line, respectively, with Mn|NbSe₂ in place of Co|NbSe₂. The dashed hexagons mark the same regions as in Fig. 2 (see caption).

grouped according to the symmetry of their structures and charge densities, and named HX-S and HX-A, for symmetric and asymmetric ones, respectively. The T-C CDW solutions are found only mixed (with the HX-A CDW). The HX-S, HX-A and T-U CDWs structures are shown in figures 3(a), (b) and (c), respectively. The HX-S features the characteristic hexagonal patches of the pristine HX CDW together with a tri-fold symmetric star of Nb-Nb bonds, compare Figs. 3(a) and 1(c). Their charge

density distributions are not remarkably different from their pristine counterparts, compare figures 3(d) and 1(f). The flatness of the (multi-dimensional) potential energy surface allows adsorption on different sites of the underlying CDW structure to give different solutions. As TABLE II reports, the HX-A CDW results from the relaxation of the adsorption of Co on the vertex of the large triangle of a T-C CDW structure, compare Fig. 1(b), and a mixing between the T-C and the HX CDWs occurs.

TABLE III. Energetics and magnetism for $M|\text{NbSe}_2$ ($M = \text{Co}, \text{K}, \text{Ga}, \text{Mn}$). Energies are given as differences with respect to the lowest energy solution and are expressed in meV; magnetic moments are expressed in μ_B .

		μ^{TM}	μ_{tot}	E^{ad}
Co	T-U	1.9	2.0	3.440
	HX-A	1.9	2.0	3.504
	HX-S	1.9	1.9	3.504
Mn	T-U	4.4	4.4	2.472
	HX-A	4.4	4.4	2.559
	HX-S	4.4	4.3	2.561
K	T-Uh	0.0	0.0	3.045
	T-UN	0.0	0.0	3.038
	HX-S	0.0	0.1	3.060
Ga	T-U	0.0	0.0	2.907
	HX-A	0.0	0.0	2.946
	HX-S	0.0	0.0	2.944

The patches in the charge density distribution, Fig. 3(e), recall those in both the pristine T-U and the pristine T-C, figs 1(e and f), supporting the previous observation. Finally, the structure and charge density distribution of the T-U solution are virtually identical to those in the pristine T-U CDW, with minor differences around the adsorption site, compare Fig. 3(f) and Figs. 1(a).

The magnetic density distributions exhibit antiferromagnetic coupling between Co and Nb in the occupied Nb band; moreover the magnetisation around Co in that energy range is opposite to the total magnetisation on Co, compare Fig. 4, first row, with TABLE III. The magnetic moment on Co (value integrated over all the occupied states) is around $2.0 \mu_B$ for every CDW, and the total magnetisation over the whole NbSe_2 layer vanishes. The same observation is valid for Mn, see TABLE III, and the discussion in the Appendix. The modulation of the magnetisation density in the HX-A CDW is larger than that in the HX-S (and that in T-U) CDW, compare Figs. 4(a and b), first row, suggesting that larger mixing of different CDWs supports the formation of a spin density wave (SDW). Moreover, a different modulation of the magnetisation densities of $\text{Co}|\text{NbSe}_2$ T-U with Co at different adsorption CDW site is observed, compare Figs. 4(c and d). These two structures are at the same energy, suggesting that a magnetic order transition is still incipient. The magnetisation data obtained by a site-by-site analysis point to a ferromagnetic coupling, in agreement with ref. [62], where an incipient magnetic transition is achieved by tensile strain.

By analysing the difference in the charge density distribution between $\text{Co}|\text{NbSe}_2$ CDWs and the pristine CDWs in the direct space, the variation of the charge modulation is studied. In the relative plots, blue (red) lobes

denote injection (depletion) of charge with respect to the pristine CDW charge distribution. The adsorption of Co modifies the T-U CDW only in the neighbourhood of the adsorption site, see Fig. 5(a), as expected from Fig. 3(f); charge depletion (injection) occurs out-of-plane (in-plane) in correspondence to the Nb at the adsorption site and in a more complex pattern on the surrounding Nb atoms; in general, red lobes point towards the adsorbate. The charge difference between the HX-A and the T-U CDWs features a constant charge difference - due to the misalignment between the two charge densities (in NbSe_2 and $\text{Co}|\text{NbSe}_2$) - and an enhancement of in-plane modulations identified by the isolated blue lobes in Fig. 5(b); these may be more relevant in comparison to the out-of-plane modulations represented by the out-of-plane red lobes on isolated Nb atoms in Fig. 5(c), which refer to Mn-adsorbed NbSe_2 .

Eliminating charge displacements (due to the different adsorption sites) helps analysing the symmetry of the charge distribution. In order to help the eye to compare the case with adsorption with the pristine case, the marks of Bragg peaks, CDW peaks and the region corresponding to points in the direct space beyond the supercell size are used in agreement with Fig. 2. The general aspect of the FT plots is virtually unchanged with respect to the pristine NbSe_2 , Fig. 2, and no difference between them can be noticed; therefore, their FT differences are shown instead. Figure 6 (a), (b) and (c) show the FT of the difference between the HX-A charge density and the pristine T-U, T-C and HX charge density, respectively; Fig. 6 (d) shows the FT of the difference between the HX-S charge density and the pristine T-U charge density, and finally (e) and (f) show the FT of the difference between the T-U CDW and the pristine T-U and T-C, respectively. All FT difference plots have a large peak around $|\mathbf{q}| = 0$ because of the background charge (uniformly) injected into the system. The symmetry is reduced in both the $\text{Co}|\text{NbSe}_2$ HX-A and T-U, as figures (a)-(c) and (e)-(f) show. Additionally, comparison of Figs. (b and c) highlights a similarity between the pristine HX and the pristine T-C CDW, mirroring the similarity of the configuration of the charge density patches, centred in the HX and T-C CDWs and non-centred in the T-U CDW. The CDW signal decreases (increases) at $|\mathbf{q}| = \frac{2\pi}{3a}$ ($|\mathbf{q}| \sim \frac{\pi}{a}$) with different magnitude along different directions in the HX-A CDW, see Figs. 6(a, d, g and j). On the other hand, the CDW signal increases at $|\mathbf{q}| \sim \frac{2\pi}{4a}$, but without a leading \mathbf{q} -vector. Furthermore, the T-U and the T-C CDW intensities change by Co adsorption: they are enhanced at different points on different hexagons, which are rotated with respect to each other by $\pi/6$, compare Figs. 6(e and f). The symmetry of the $\text{Co}|\text{NbSe}_2$ HX-A and T-U is the same (C_2), suggesting that, even for lower concentration, where the energy competition starts to turn in favour of the T-U CDW, the symmetry of the charge density distribution is likely reduced (from C_6 to C_2). As Co adsorption on a $9 \times 9 \times 1$ supercell was investigated, the gap between the T-U and HX-A CDWs

decreases to 0.3 meV/f.u. still in favour of the latters, pointing to a trend which likely favours the T-U CDW in smaller concentrations. Likely, thermal fluctuations are going to make these different CDWs available; nevertheless, their hierarchy is clarified. Four solutions, two for each CDW family, are shown in Fig. 13 in Appendix.

B. Adsorption of Mn

Moving to the case of Mn adsorption, we first notice that the magnetism plays a major role in the modelling of the systems. In particular, a high magnetic moment, which correctly describes Mn, favours the Nb site more than in the case of Co adsorption (the energy difference between the Nb site and the hollow site is 5 times larger), compare their energy differences in TABLE I. The ordering of the CDW structures, assessed by total energy calculations, follows the same pattern as in the case of Co adsorption, having a family of ground state HX CDWs, including a symmetric one and an asymmetric one, a solution of T-U at a higher energy and the absence of a T-C solution. The energy difference between the ground state HX CDW and the T-U solution is 1.5 meV/f.u., see TABLE II, which compared to the case of Co, it suggests that Mn drives a slightly stronger transition to a HX CDW. The charge density distributions of the HX-S and HX-A show no essential difference, being also very similar to that of Co|NbSe₂ HX-S. Therefore, the relative figures are omitted, and the remaining discussion is limited to the magnetisation density distributions and the FT of the charge density distributions.

The magnetisation densities of the HX-S, HX-A the T-U are shown in Fig. 4, second row. The two HX CDWs are similar also in their magnetisation density distribution - compare with the case of Co adsorption, Fig. 4, second row. The structure of HX-A has a reflection symmetry through the top-left to bottom-right diagonal as represented in Fig. 4. The T-U CDW structure is modified slightly in the vicinity of the adsorption site. The magnetisation density in all of the CDWs is negative around Mn, unlike the case of Co, where a negative cloud surrounding Co is neighboured by a positive cloud around the closest Nb atoms, compare also Figs. 15(a and b) in the Appendix, showing a detailed view on the vicinity of the adsorption sites.

Charge density differences in direct space are analysed in comparison with Co adsorption. The main difference between the two adsorbates is that with Mn adsorption the out-of-plane charge modulations are not suppressed. In fact, note that the in-plane red lobes in Fig. 5(e) replace the out-of-plane red lobes in Fig. 5(c), point in three directions, symmetrically. In fact, the similarity between Figs. 5(d and f) confirms that the HX-S has the same features in the case of Co and Mn, with blue lobes pointing out-of-plane.

The FT analysis is analogous to the case of Co; Fig. 6 shows the following set of FT difference of the charge dis-

tributions: ground state HX-A minus T-U, T-C and HX, respectively (a), (b) and (c); ground state HX-S minus T-U (d), T-U minus T-U (e) and T-C (f). The general qualitative picture seen for the charge density distribution upon Co adsorption, which consists of a symmetry reduced from C_6 to C_2 in the HX-A CDW and in the T-U CDW, is valid for Mn adsorption as well. However, the intensity variation in the FT plots is smaller in the case of Mn adsorption, showing little contrast between the C_6 and the C_2 symmetries, compare the HX-A and HX-S CDWs in Figs. 6(g and j) with the T-U CDWs in Fig. 6(e) and Fig. 6(k). The preference for the TM for the HX CDWs seems to be at variance with their tendency of inducing a C_6 to C_2 symmetry transition. The lowest energy solutions for Co|NbSe₂ (and Mn|NbSe₂) are mixed state of HX and T-C CDWs, compare Fig. 3(b) with Fig. 1(b). However the Co|NbSe₂ HX-A CDW solution has a consistent T-C component, whereas the Mn|NbSe₂ HX-A CDW solution has a small T-C component, see the underlying structure in the magnetisation density plot, Fig. 4(e). In summary, the CDW solutions for TM adsorbates on NbSe₂ are mixed states; where the mixing between HX and T-C is high, the symmetry of the charge density distribution is reduced, whereas predominant HX CDW solutions keep a C_6 symmetry. In the case of Mn, the preference for HX solutions is higher than in the case of Co, and as a result the T-C component in the mixed solutions is smaller and in turn the C_6 symmetry is virtually maintained. Finally, the observation that the T-U / T-C have a reduced symmetry, raises the question on pristine T-U/C and the symmetry of its charge density distribution, which has a C_6 symmetry; perhaps the adsorbates induces some symmetry breaking which allows the T-U to undergo a transition.

Table IV shows the occupancies of Co and Mn 3d orbitals. The environment around the TM in the NbSe₂ layer is trigonal prismatic, and therefore orbitals split into three groups due to the crystal field; these are classified according to their symmetry into e'' , e' and a'_1 . The orbital splitting is valid also for Co and Mn 3d orbitals, but the intensity of the splitting is reduced because the environment is incomplete. Therefore, the spin splitting, which depends on the l -character of the orbitals is larger than or comparable to the crystal field splitting, and orbitals are ordered by increasing energy as follows: in the majority spin channel, e'' , e' and a'_1 ; in the minority spin channel the order to e' and a'_1 is inverted. Furthermore, the orbital projections onto the conventional basis (xy , yz , $d_{z^2-3r^2}$, zx and $d_{x^2-y^2}$, ordered by increasing m value) are spin dependent. The orbitals of the eigenbasis can be written as $e''^1_\sigma = v_\sigma d_{xy} + u_\sigma d_{yz}$, $e''^2_\sigma = u_\sigma d_{zx} + v_\sigma d_{x^2-y^2}$, $e'^1_\sigma = u_\sigma d_{xy} + v_\sigma d_{yz}$ and $e'^2_\sigma = v_\sigma d_{zx} + u_\sigma d_{x^2-y^2}$. (Freedom in the choice of the basis set allows one to set $a'_1 = d_{z^2-3r^2}$.) The l -character of the e'^\uparrow orbitals is close to 1 (i.e. the u values are larger than the v values); conversely, the e'^\uparrow orbitals have a prevalent $l = 2$ character (v values are larger); overall,

this fact holds for the $e''\downarrow$ and $e'\downarrow$ orbitals.

In summary, TM adsorption favours HX CDW, weakening the CDW signals for the T-U and T-C CDWs, and the symmetry of the charge distribution is reduced from C_6 to C_2 , especially in the case of Co, where mixing between HX and T-C occur. The modulation of the magnetic density is dependent on the symmetry of the charge distribution: the higher the symmetry, the weaker the modulation. Also, due to a weaker crystal field splitting, the orbital order of the $3d$ of Co and Mn in the two spin channels is different. Finally, a probe for Mn and Co is given in terms of l -character of their electrons.

C. Adsorption of K and Ga

The hollow adsorption site on a non modulated NbSe₂ structure stands 4 meV above the Nb adsorption site, hence being more competitive with respect to the other adsorbates considered (with the exception of a low-spin solution for Mn which favours the hollow site, but which was discarded because it is unphysical or unlikely to occur). When modelling the adsorption on the CDW modulated structures, the energy difference between the two sites become 0.2 meV/f.u. in favour of the hollow site. The solutions obtained starting from the T-C converge to mixed states between T-C itself and HX and they are found at a high energy, while the T-U CDW is still favoured by 0.7 meV/f.u. over the HX CDW (the energy difference slightly changes with respect to the pristine case). The CDW structure and charge density distribution in the T-U on the hollow site (the ground state) and in the T-U on the Nb site look very similar, see Fig. 7. The FT analysis shows slight differences: the FT difference between K[NbSe₂] with K adsorbed on a Nb site and the pristine case slightly differ from a C_6 symmetry for small values of $|\mathbf{q}|$, see Fig. 8; however, the difference in intensity is one order of magnitude smaller than that of the Nb and Mn cases.

The case of Ga is interesting to compare with K because it is an atom with a fully occupied s orbital and a single electron in the p orbital. In this case, the adsorption on the Nb site is favoured by 183 meV. over the adsorption at the hollow site. The T-U CDW is in strong competition or coexists with the HX CDW, and the T-C converges to a mixed solution between T-C and HX, analogously to the case of K. The ground state structures are shown in Fig. 7. The charge density distributions are their FTs are not particularly different from the case with K adsorption.

Overall, adsorption of atoms on NbSe₂ single layers suppresses the T-C CDW and promotes the HX CDWs in all cases; in particular, with Co and Mn the HX CDWs become the ground state for all the coverage considered in this study, whereas in the case of Ga the HX CDWs are at the same energy of the T-U CDW. Adsorption of K does not change the ground state but does suppress the T-C CDW; the HX CDWs are the closest ones to the ground

state, within thermal fluctuations (at 0.7 meV/f.u.) and therefore very likely to be seen by Scanning Tunnelling Microscopy in real samples. In fact, as several STM data are becoming available, a guide on the CDW hierarchy may be very useful to correctly identify and locate metallic impurities in TMDCs. Furthermore, the symmetry of the charge density distribution is reduced from C_6 to C_2 , hinting to a weakening of a \mathbf{q} -vector, which may be the precursor of a stripe phase recently observed by STM [48, 49].

TABLE IV. Occupancies on Co and Mn $3d$ orbitals, which split according to a trigonal prismatic environment, namely e'' , e' and a'_I , where $a'_I = d_{z^2-3r^2}$. The coefficients u_\uparrow , v_\uparrow , u_\downarrow and v_\downarrow are .90, .43, .62 and .78 for Co and .99, .16, .78 and .62 for Mn, respectively.

	Co		Mn	
	$\sigma = \uparrow$	$\sigma = \downarrow$	$\sigma = \uparrow$	$\sigma = \downarrow$
$e'_{I,\sigma}$	0.93	0.07	0.93	0.03
a'_I	0.90	0.79	0.92	0.08
$e''_{I,\sigma}$	0.95	0.92	0.93	0.09

V. CONCLUSIONS

By means of *ab-initio* calculations based on total energy and direct space charge computation, we have investigated the existence and competition of CDWs in single layer NbSe₂ without and with impurities. The T-C CDW is suppressed in all cases, suggesting that its observation in STM images is unlikely in non-passivated samples, due to the high reactivity of NbSe₂ and, in general, metallic TMDCs. Transition metal adsorbates invert the energy hierarchy between CDWs, favouring the HX CDWs over the T-U and the T-C. Adsorption of K keep the T-U CDW as the ground state, although the HX CDW is preferred to the T-C CDW; adsorption of Ga equally favours the T-U and the HX CDWs pointing to a coexistence. In general, adsorption of atoms, changing the local symmetry mixes the ‘pristine’ CDWs, in particular the HX and the T-C. The symmetry of the charge density distribution is reduced from C_6 to C_2 upon Co or Mn adsorption.

ACKNOWLEDGEMENTS

We are grateful to B. I. Min and V. Fiorentini for fruitful discussions. This work is supported by Basic Science Research Programs (2015R1C1A1A01052411) and (2017R1D1A1B03033465) through the National Research Funding Agency of the Republic of Korea (NRF) funded by the government of the Republic of Korea (MSIP). K. K. and A. A. acknowledge the Max Planck POSTECH / KOREA Research Initiative (No. 2011-0031558) programs through NRF funded by MSIP of Korea. The computational work was performed on resources provided by the Swedish National Infrastructure for Com-

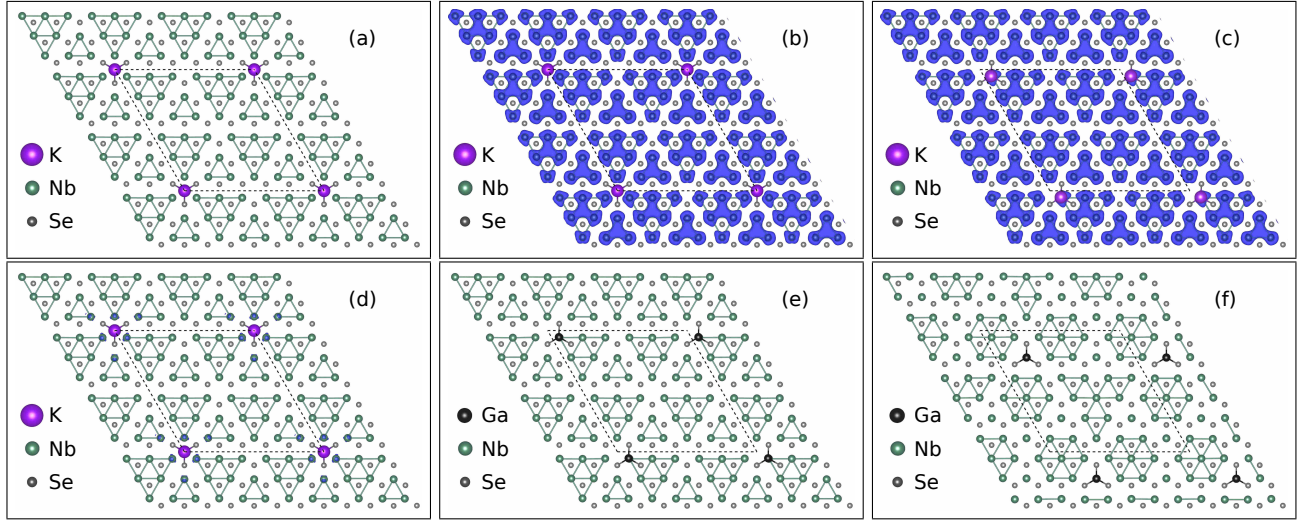


FIG. 7. (Colour online) First row: ground state CDW structure, with K adsorbed on the hollow position (a), its charge density distribution (b), and the charge density for K adsorbed on the Nb site (c); Second row: Difference in the charge densities between the K[NbSe₂] ground state and NbSe₂ T-U (d), ground state CDW structures for two Ga[NbSe₂], namely T-U (e) and HX-A (f). Atoms are represented by spheres, as illustrated in the legends; Nb-Nb bonds shorter than the equilibrium distance (3.45 Å) are represented by solid lines to help visualising the CDW structure pattern. Dashed lines mark the supercells borders. The isosurface value for the volumetric data is set in agreement with Fig. 1.

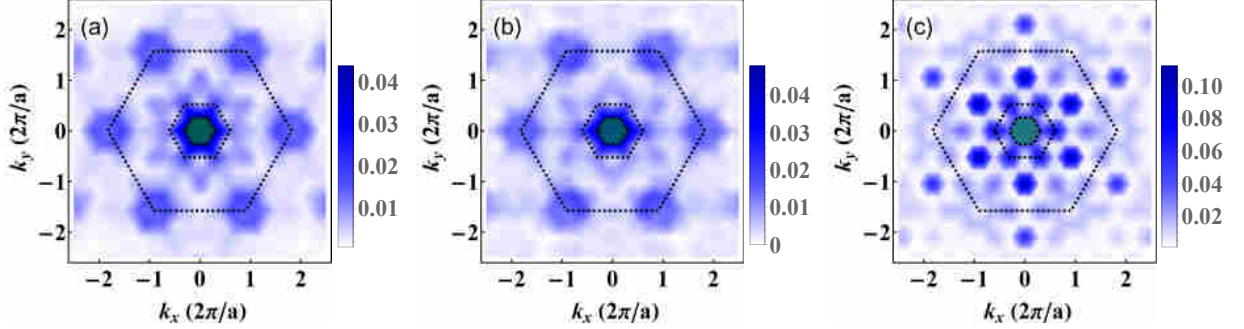


FIG. 8. (Colour online) Difference in the FT of the charge density distributions between the K[NbSe₂] on the hollow site (a), and Nb site (b) and the T-U pristine CDW. The charge distribution has a C_2 symmetry for the adsorption on the hollow site and a C_6 symmetry for the adsorption on the Nb site. In (c), the FT difference between K[NbSe₂] on the hollow site and the pristine T-C CDW is shown.

puting (SNIC) at the High Performance Computing Center North (HPC2N) and at the National Computational Infrastructure (NCI) of Australia. We also acknowledge the IBS centre at POSTECH and the Korean Institute of Science and Technology Information (KISTI).

Appendix A: Pristine

As reported in the literature, the (multi-dimensional) potential energy surface of the CDW phase features several (rather shallow) minima; as a result, several symmetries are possible. The existence of two forms of orthorhombically distorted structures was mentioned in the main text, and is extensively explained in the literature. Some differences identified in the main text included the

mention of the accompanying Se-Se bonds. Figure 9(a, b and c) show the T-U, T-C and HX CDWs respectively, highlighting their Se-Se distance patterns. Also hexagonally distorted structures can exist in two forms, one having hexagonal Nb-Nb patterns, analysed throughout the manuscript, and one having three-fold symmetric Nb clusters, as shown in Fig. 11. This latter structure does not converge within our $6 \times 6 \times 1$ supercells, and appears to be stabilised only in a $9 \times 9 \times 1$ supercell; it is found at a higher energy with respect to the other three CDW structures (2.7 meV above the T-U CDW structure) and therefore further analysis has been dismissed; its structure is shown in two figures, 11(a) and (b), with its Nb clusters and its Se clusters, respectively.

With reference to Fig. 10, the DOS of the main three CDW structures are compared to the DOS of the fully

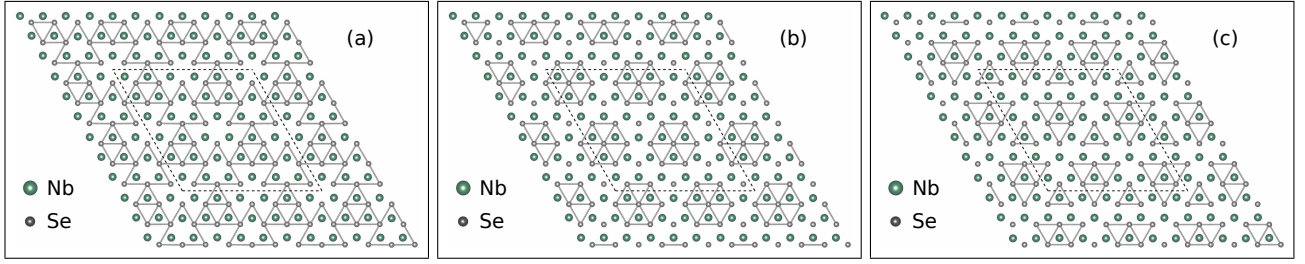


FIG. 9. (Colour online) Relaxed structures of the pristine CDWs as they appear in Fig. 1 in the main text: T-U (a), T-C (b) and HX (c). Atoms are represented by spheres, as illustrated in the legends; Se-Se bonds shorter than the equilibrium distance (3.45 Å) are represented by solid lines, in order to help visualising the CDW structure pattern. Dashed lines mark the supercells borders.

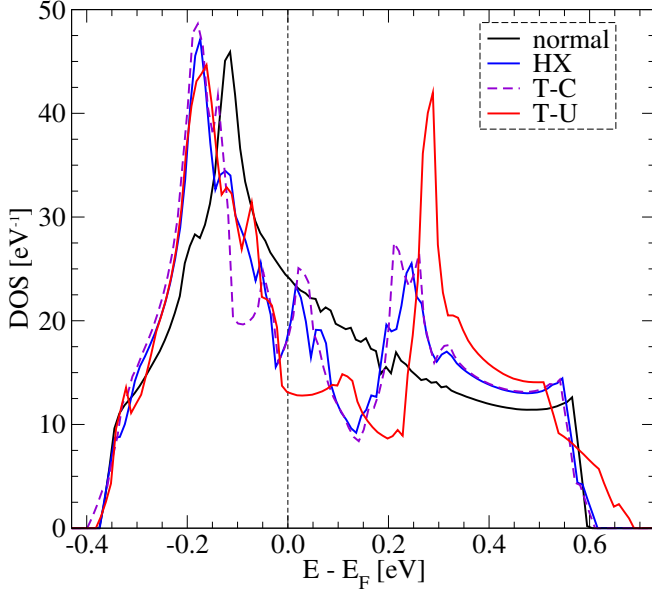


FIG. 10. (Colour online) Total DOS of NbSe₂ with the fully symmetric structure and with the HX, the T-C and the T-U CDW structures, obtained for a $3 \times 3 \times 1$ supercell.

symmetric structure of pristine NbSe₂. As presented elsewhere [38], for single layers a single band crosses the Fermi level and extends from ~ -0.4 eV to $\sim +0.7$ eV. As the main contribution for this band come from Nb states, we refer to such band as Nb band. The CDW formation shifts the spectral weight from ~ -0.10 eV to ~ -0.20 eV and enhances it in the range $(+0.25, +0.30)$ eV; the DOS peaks are aligned around -0.20 eV, whereas the DOS peaks around $+0.25$ eV are at different energy for different CDWs. The T-U CDW DOS features a depletion of spectral weight in correspondence of the Fermi level till $\sim +0.10$ eV and a trough at $\sim +0.20$ eV (which in fact precedes the peak at $\sim +0.30$ eV); the T-C CDW DOS has a trough at ~ -0.10 eV, a second one at Fermi level and a third one at $\sim +0.15$ eV; the HX CDW DOS has one trough at Fermi level and one at $\sim +0.15$ eV, being more similar to the T-C CDW DOS. The T-U differs from the other two also by a slightly larger band-width,

whose tail reaches ~ 0.7 eV. Overall, the CDW affects different energy ranges of the DOS both around the Fermi level and away from it, in agreement with the literature [38, 59].

Appendix B: Co adsorption

A single Co adsorbed on NbSe₂, with a concentration of 1 atom over 81 unit cells, was studied in order to assess how fast the energy order changes to recover that of pristine system. The structure of the HX solutions shows some similarities to the case with higher adsorbate coverage. No T-C CDW was found among the low energy solutions, whereas solutions consisting of HX mixed with T-C are present, see Figs. 13(a and c). The T-U solutions are closer in energy to the ground state solution HX-A (0.3 meV/f.u.), whereas mixed CDWs are found at higher energy, Figs. 13(b and d), respectively.

The direct space charge distribution of two solutions, the lowest energy HX solution and the first T-U solution, is shown in Figs. 14(a and b), corresponding to the structures shown in Figs. 13(a and b); the HX solution shows characteristic patches of the T-C and HX CDWs, following the structural modulation and confirming the tendency for these two CDW to mix together upon Co adsorption; in fact, patches as represented in Fig. 1 are found in the $9 \times 9 \times 1$ supercell. The charge distribution of the T-U solution looks almost identical to that in the $6 \times 6 \times 1$ supercell, including the reduced symmetry, which is likely due to unidirectional local structural distortions driven by the Co electronic degree of freedom.

Finally, the DOS of symmetric and selected CDW structures obtained in the $6 \times 6 \times 1$ supercells was computed and analysed for Co|NbSe₂ and for K|NbSe₂, see Fig. 12. By relaxing the M|NbSe₂ (M = Co, K) structures fixing the in-plane coordinates of the Nb and Se atoms, the symmetry of each structure has been preserved. The main features of the DOS of the T-U and HX CDWs are maintained with respect to the pristine CDWs: the position of the peaks at ~ -0.20 eV and $\sim +0.25$ eV, and the depletion of states around Fermi level. However, while the depletion of states in the pristine HX CDW is

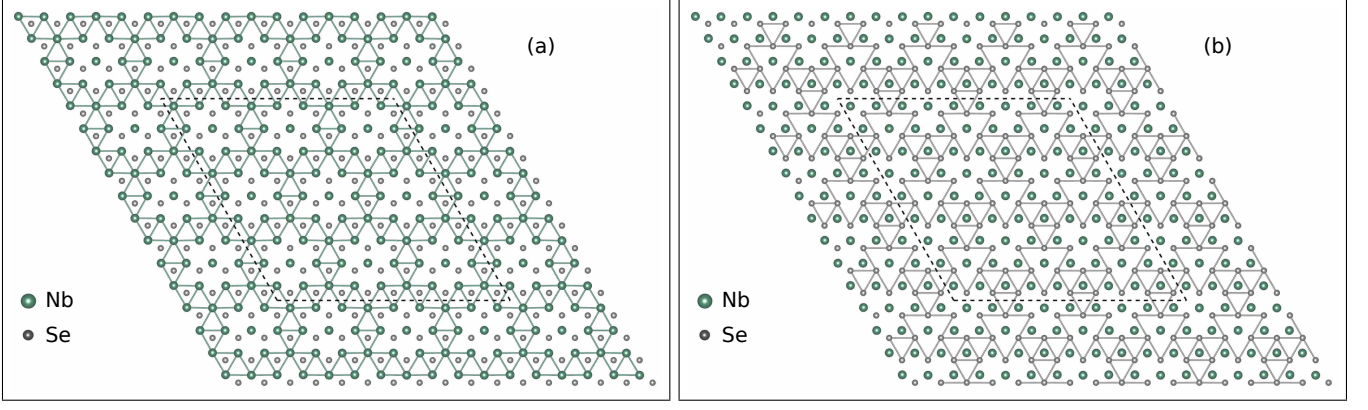


FIG. 11. (Colour online) Relaxed structures of a variant of the HX CDW in a $9 \times 9 \times 1$ supercell, highlighting its Nb-Nb (a) and Se-Se (b) distance pattern. Atoms are represented by spheres, as illustrated in the legends; in (a) and (b) respectively, Nb-Nb or Se-Se bonds shorter than the equilibrium distance (3.45 Å) are represented by solid lines, in order to help visualising the CDW structure pattern. Dashed lines mark the supercells borders.

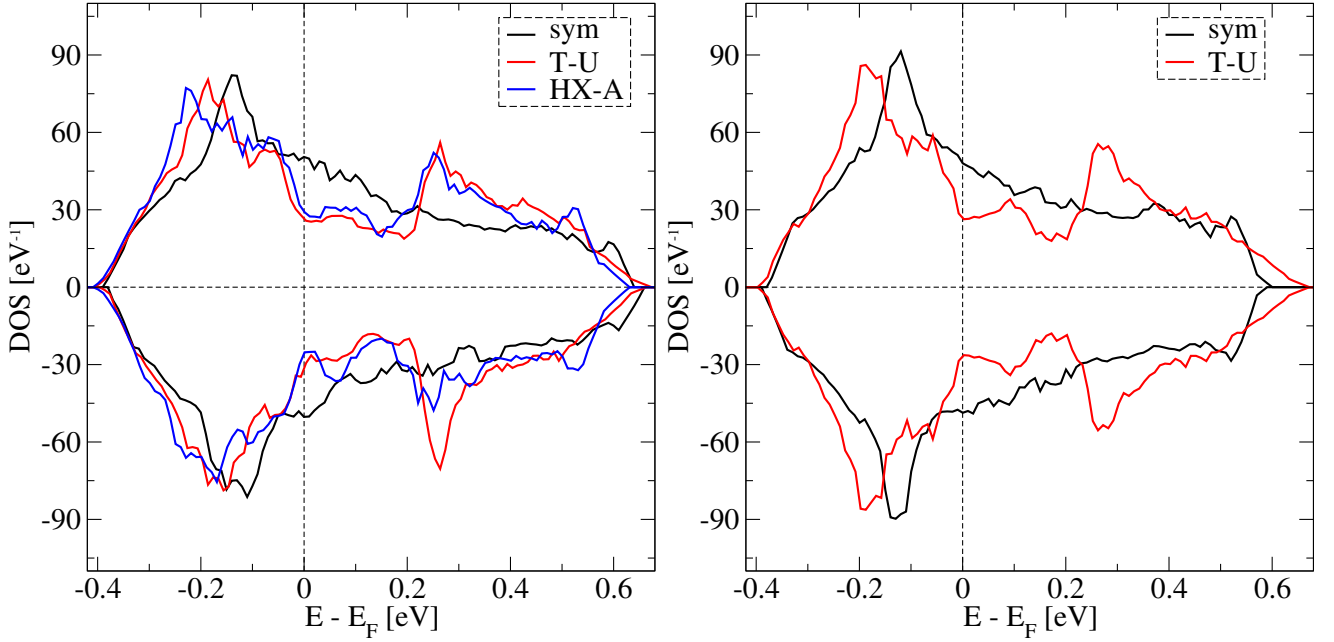


FIG. 12. (Colour online) Total DOS of Co|NbSe₂ and K|NbSe₂ with symmetric structures and with their CDW structures.

accompanied by peaks and troughs near Fermi level, the depletion of states in the HX-A CDW (i.e. with Co adsorbates) shows a more consistent profile. In summary, the effect of the CDW on the DOS slightly differs passing from the pristine case to the case with adsorbates, the states around Fermi level being the most affected ones.

Appendix C: Magnetic density

The comparison between magnetic couplings within the Nb band in the two cases of Co adsorption and Mn

adsorption has been discussed in the main text. The actual magnetic moments (i.e. involving all states up to Fermi level) of Co, Mn and their respective underlying Nb atoms read $+1.9\mu_B$, $+4.4\mu_B$, $+0.6\mu_B$ and $-0.8\mu_B$, respectively. In summary, the Co and Mn magnetic moments in the Nb bands are inverted with respect to the total magnetic moments, while the underlying Nb magnetic moments do not change sign, remaining positive in the case of Co adsorption and negative in the case of Mn adsorption.

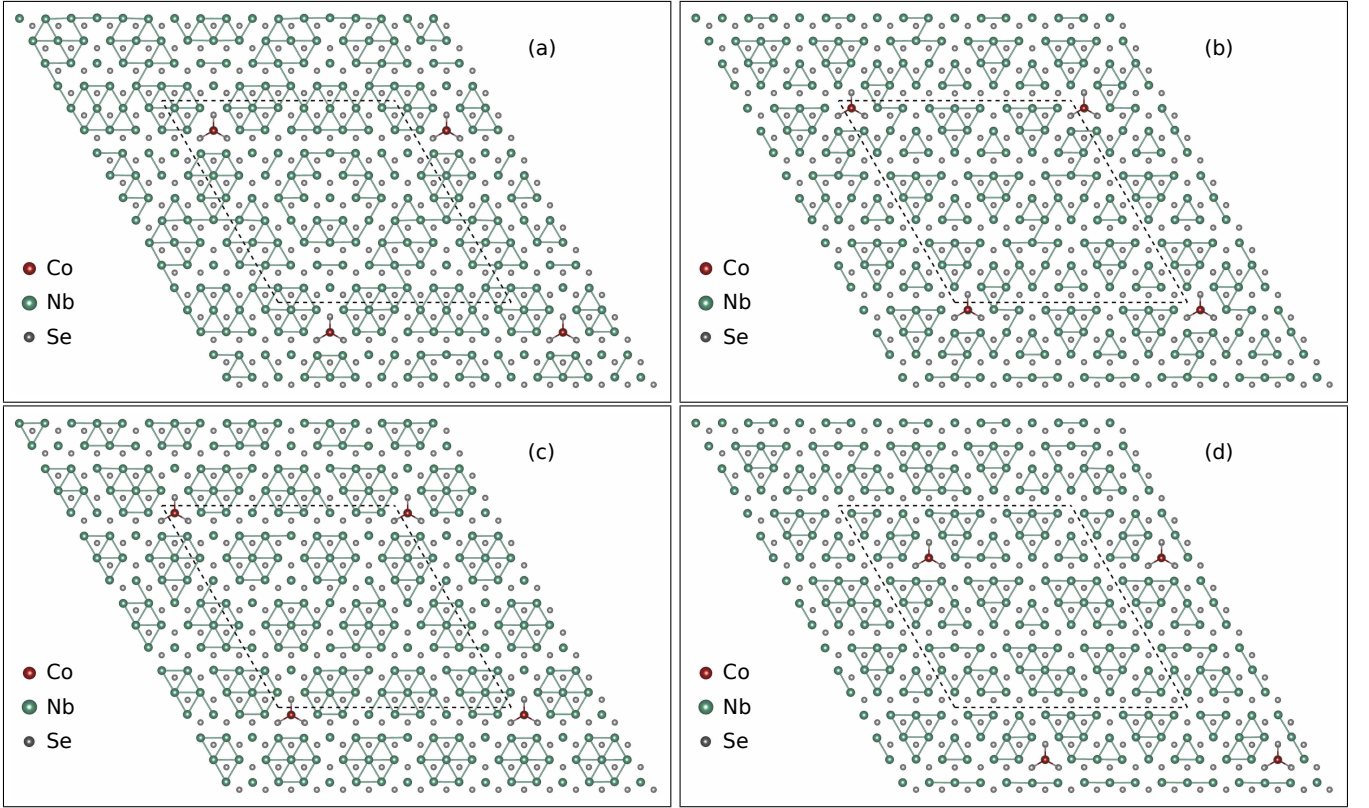


FIG. 13. (Colour online) Relaxed structures of $\text{Co}[\text{NbSe}_2]$ in a $9 \times 9 \times 1$ supercell. Atoms are represented by spheres, as illustrated in the legends; Nb-Nb bonds shorter than the equilibrium distance (3.45 \AA) are represented by solid lines, in order to help visualising the CDW structure pattern. Dashed lines mark the supercells borders.

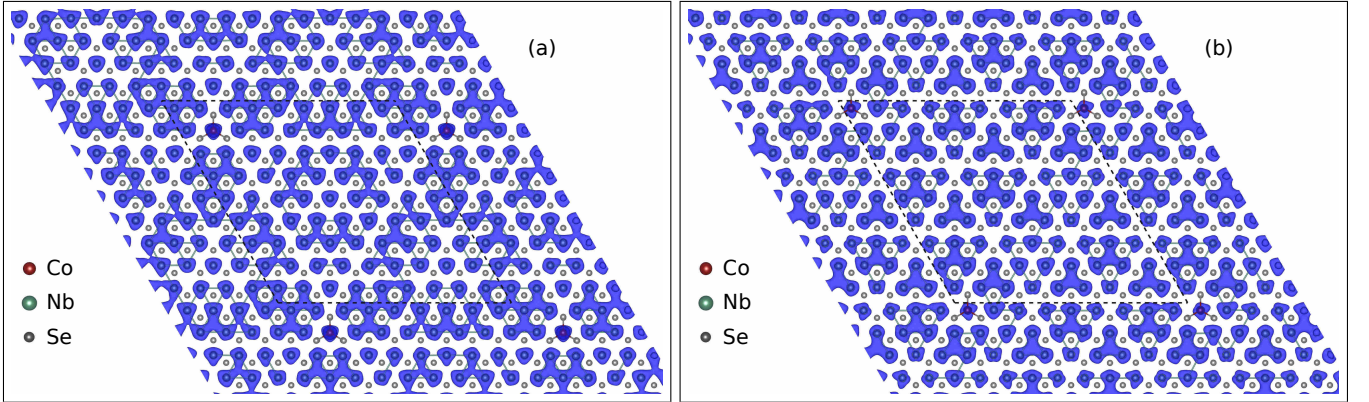


FIG. 14. (Colour online) Direct space charge density distribution of $\text{Co}[\text{NbSe}_2]$ in a $9 \times 9 \times 1$ supercell; (a) and (b) correspond to the respective structures in Fig. 13. The isosurface value for the volumetric data is set in agreement with the relative figures in the main text. Atoms are represented by spheres, as illustrated in the legends; Nb-Nb bonds shorter than the equilibrium distance (3.45 \AA) are represented by solid lines, in order to help visualising the CDW structure pattern. Dashed lines mark the supercells borders.

-
- [1] K. S. Novoselov, D. Jiang, F. Schedin, T. J. Booth, V. V. Khotkevich, S. V. Morozov, and A. K. Geim, *Proc. Natl. Acad. Sci. U.S.A.* **102**, 10451 (2005).
- [2] M. Xu, T. Liang, M. Shi, and H. Chen, *Chem. Rev.* **113**, 3766 (2013).
- [3] W. Choi, N. Choudhary, G. H. Han, J. Park, D. Akinwande, and Y. H. Lee, *Mater. Today* **20**, 116 (2017).

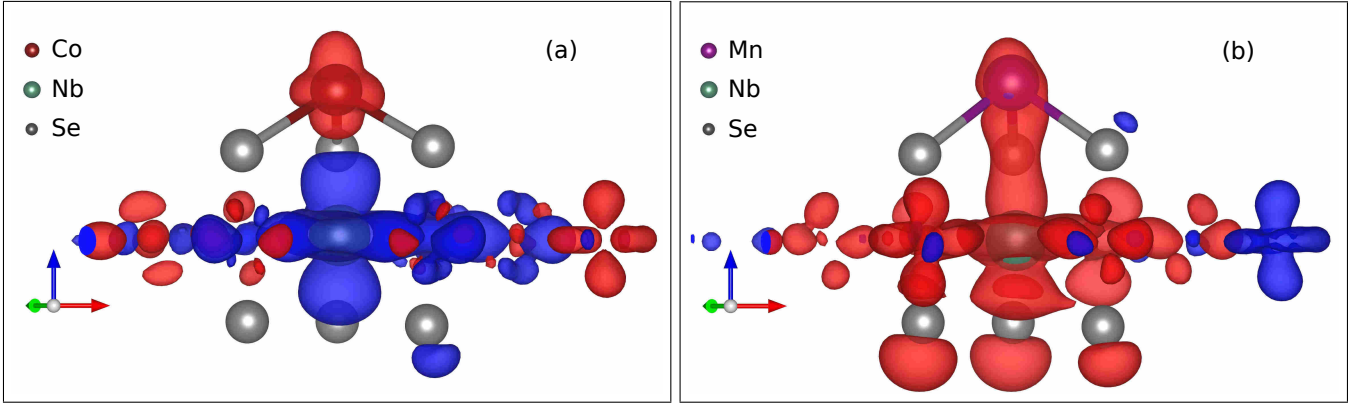


FIG. 15. (Colour online) Magnetisation densities of Co[NbSe₂] T-U (a) and Mn[NbSe₂] T-U (b) with details around Co and Mn, respectively. The sets of axes represent the unitary lattice vectors in red, green and blue colour, respectively. Volumetric data representation are set in agreement to the relative figures in the main text.

- [4] S. Z. Butler, S. M. Hollen, L. Cao, Y. Cui, J. A. Gupta, H. R. Gutiérrez, T. F. Heinz, S. S. Hong, J. Huang, A. F. Ismach, E. Johnston-Halperin, M. Kuno, V. V. Plashnitsa, R. D. Robinson, R. S. Ruoff, S. Salahuddin, J. Shan, L. Shi, M. G. Spencer, M. Terrones, W. Windl, and J. E. Goldberger, *ACS Nano* **7**, 2898 (2013).
- [5] A. K. Geim and I. V. Grigorieva, *Nature* **499**, 419 (2013).
- [6] K. S. Novoselov, A. Mishchenko, A. Carvalho, and A. H. Castro Neto, *Science* **353**, 461 (2016).
- [7] A. Splendiani, L. Sun, Y. Zhang, T. Li, J. Kim, C.-Y. Chim, G. Galli, and F. Wang, *Nano Lett.* **10**, 1271 (2010).
- [8] K. F. Mak, C. Lee, J. Hone, J. Shan, and T. F. Heinz, *Phys. Rev. Lett.* **105**, 136805 (2010).
- [9] A. Kuc, N. Zibouche, and T. Heine, *Phys. Rev. B* **83**, 245213 (2011).
- [10] Q. H. Wang, K. Kalantar-Zadeh, A. Kis, J. N. Coleman, and M. S. Strano, *Nat. Nanotechnol.* **7**, 699 (2012).
- [11] M. Chhowalla, H. S. Shin, G. Eda, L.-J. Li, K. P. Loh, and H. Zhang, *Nat. Chem.* **5**, 263 (2013).
- [12] R. F. Frindt, *Phys. Rev. Lett.* **28**, 299 (1972).
- [13] J. A. Wilson, F. J. D. Salvo, and S. Mahajan, *Advances in Physics* **50**, 1171 (2001).
- [14] Z. R. Gong, W. Z. Luo, Z. F. Jiang, and H. C. Fu, *Sci. Rep.* **7**, 42390 (2017).
- [15] Y. Qi, P. G. Naumov, M. N. Ali, C. R. Rajamathi, W. Schnelle, O. Barkalov, M. Hanfland, S.-C. Wu, C. Shekhar, Y. Sun, V. Süß, M. Schmidt, U. Schwarz, E. Pippel, P. Werner, R. Hillebrand, T. Förster, E. Kampert, S. Parkin, R. J. Cava, C. Felser, B. Yan, and S. A. Medvedev, *Nat. Commun.* **7**, 11038 (2016).
- [16] X. Xi, L. Zhao, Z. Wang, H. Berger, L. Forró, J. Shan, and K. F. Mak, *Nat. Nanotechnol.* **10**, 765 (2015).
- [17] X. Xi, Z. Wang, W. Zhao, J.-H. Park, K. T. Law, H. Berger, L. Forró, J. Shan, and K. F. Mak, *Nat. Phys.* **12**, 139 (2016).
- [18] M. M. Ugeda, A. J. Bradley, Y. Zhang, S. Onishi, Y. Chen, W. Ruan, C. Ojeda-Aristizabal, H. Ryu, M. T. Edmonds, H.-Z. Tsai, A. Riss, S.-K. Mo, D. Lee, A. Zettl, Z. Hussain, Z.-X. Shen, and M. F. Crommie, *Nat. Phys.* **12**, 92 (2016).
- [19] X. Xi, H. Berger, L. Forró, J. Shan, and K. F. Mak, *Phys. Rev. Lett.* **117**, 106801 (2016).
- [20] X. Zhu, Y. Guo, H. Cheng, J. Dai, X. An, J. Zhao, K. Tian, S. Wei, X. Cheng Zeng, C. Wu, and Y. Xie, *Nat. Commun.* **7**, 11210 (2016).
- [21] A. J. Bevelo and H. R. Shanks, *J. Appl. Phys.* **45**, 4644 (1974).
- [22] R. Corcoran, P. Meeson, Y. Onuki, P. A. Probst, M. Springford, K. Takita, H. Harima, G. Y. Guo, and B. L. Gyorffy, *J. Phys.: Cond. Matt.* **6**, 4479 (1994).
- [23] J. A. Wilson, F. J. Di Salvo, and S. Mahajan, *Phys. Rev. Lett.* **32**, 882 (1974).
- [24] D. E. Moncton, J. D. Axe, and F. J. DiSalvo, *Phys. Rev. Lett.* **34**, 734 (1975).
- [25] E. Revolinsky, G. A. Spiering, and D. J. Beerntsen, *J. Phys. Chem. Solids* **26**, 1029 (1965).
- [26] D. J. Rahn, S. Hellmann, M. Kalläne, C. Sohr, T. K. Kim, L. Kipp, and K. Rossnagel, *Phys. Rev. B* **85**, 224532 (2012).
- [27] A. H. Castro Neto, *Phys. Rev. Lett.* **86**, 4382 (2001).
- [28] J. A. Galvis, E. Herrera, C. Berthod, S. Vieira, I. Guillelmon, and H. Suderow, *Communications Physics* **1**, 30 (2018).
- [29] C. J. Arguello, E. P. Rosenthal, E. F. Andrade, W. Jin, P. C. Yeh, N. Zaki, S. Jia, R. J. Cava, R. M. Fernandes, A. J. Millis, T. Valla, R. M. Osgood, and A. N. Pasupathy, *Phys. Rev. Lett.* **114**, 037001 (2015).
- [30] T. M. Rice and G. K. Scott, *Phys. Rev. Lett.* **35**, 120 (1975).
- [31] R. Liu, C. G. Olson, W. C. Tonjes, and R. F. Frindt, *Phys. Rev. Lett.* **80**, 5762 (1998).
- [32] T. Straub, T. Finteis, R. Claessen, P. Steiner, S. Hufner, P. Blaha, C. S. Oglesby, and E. Bucher, *Phys. Rev. Lett.* **82**, 4504 (1999).
- [33] D. S. Inosov, V. B. Zabolotnyy, D. V. Evtushinsky, A. A. Kordyuk, B. Büchner, R. Follath, H. Berger, and S. V. Borisenko, *New J. Phys.* **10**, 125027 (2008).
- [34] K. Rossnagel, O. Seifarth, L. Kipp, M. Skibowski, D. Voß, P. Krüger, A. Mazur, and J. Pollmann, *Phys. Rev. B* **64**, 235119 (2001).
- [35] K. Rossnagel and N. V. Smith, *Phys. Rev. B* **76**, 073102 (2007).
- [36] M. D. Johannes, I. I. Mazin, and C. A. Howells, *Phys. Rev. B* **73**, 205102 (2006).

- [37] M. D. Johannes and I. I. Mazin, *Phys. Rev. B* **77**, 165135 (2008).
- [38] M. Calandra, I. I. Mazin, and F. Mauri, *Phys. Rev. B* **80**, 241108 (2009).
- [39] T. Valla, A. V. Fedorov, P. D. Johnson, P.-A. Glans, C. McGuinness, K. E. Smith, E. Y. Andrei, and H. Berger, *Phys. Rev. Lett.* **92**, 086401 (2004).
- [40] X. Zhu, Y. Cao, J. Zhang, E. W. Plummer, and J. Guo, *Proc. Natl. Acad. Sci. U.S.A.* **112**, 2367 (2015).
- [41] V. N. Kotov, B. Uchoa, V. M. Pereira, F. Guinea, and A. H. Castro Neto, *Rev. Mod. Phys.* **84**, 1067 (2012).
- [42] F. Guinea, M. I. Katsnelson, and T. O. Wehling, *Ann. Phys. (Berl.)* **526**, A81 (2014).
- [43] K. F. Mak, K. He, C. Lee, G. H. Lee, J. Hone, T. F. Heinz, and J. Shan, *Nat. Mater.* **12**, 207 (2012).
- [44] A. Skripov and A. Stepanov, *Solid State Commun.* **53**, 469 (1985).
- [45] C. D. Malliakas and M. G. Kanatzidis, *J. Am. Chem. Soc.* **135**, 1719 (2013).
- [46] J. Ángel Silva-Guillén, P. Ordejón, F. Guinea, and E. Canadell, *2D Materials* **3**, 035028 (2016).
- [47] U. Chatterjee, J. Zhao, M. Iavarone, R. Di Capua, J. P. Castellan, G. Karapetrov, C. D. Malliakas, M. G. Kanatzidis, H. Claus, J. P. C. Ruff, F. Weber, J. van Wezel, J. C. Campuzano, R. Osborn, M. Randeria, N. Trivedi, M. R. Norman, and S. Rosenkranz, *Nat. Commun.* **6**, 6313 (2015).
- [48] A. Fang, C. Adamo, S. Jia, R. J. Cava, S.-C. Wu, C. Felser, and A. Kapitulnik, *Sci. Adv.* **4**, eaq0330 (2018).
- [49] A. Soumyanarayanan, M. M. Yee, H. Yang, v. W. Jasper, D. J. Rahn, K. Rossnagel, E. W. Hudson, M. R. Norman, and J. E. Hoffman, *Proc. Natl. Acad. Sci. U.S.A.* **110** (2013).
- [50] K. Cho, M. Konczykowski, S. Teknowijoyo, M. A. Tanatar, J. Guss, P. B. Gartin, J. M. Wilde, A. Kreyssig, R. J. McQueeney, A. I. Goldman, V. Mishra, P. J. Hirschfeld, and R. Prozorov, *Nat. Commun.* **9**, 2796 (2018).
- [51] P. E. Blöchl, *Phys. Rev. B* **50**, 17953 (1994).
- [52] G. Kresse and D. Joubert, *Phys. Rev. B* **59**, 1758 (1999).
- [53] J. P. Perdew, K. Burke, and M. Ernzerhof, *Phys. Rev. Lett.* **77**, 3865 (1996).
- [54] J. P. Perdew, K. Burke, and M. Ernzerhof, *Phys. Rev. Lett.* **78**, 1396 (1997).
- [55] T. O. Wehling, A. I. Lichtenstein, and M. I. Katsnelson, *Phys. Rev. B* **84**, 235110 (2011).
- [56] A. I. Liechtenstein, V. I. Anisimov, and J. Zaanen, *Phys. Rev. B* **52**, R5467 (1995).
- [57] J. Wilson and A. Yoffe, *Adv. Phys.* **18**, 193 (1969).
- [58] C.-S. Lian, C. Si, and W. Duan, *Nano Lett.* **18**, 2924 (2018).
- [59] D. W. Shen, B. P. Xie, J. F. Zhao, L. X. Yang, L. Fang, J. Shi, R. H. He, D. H. Lu, H. H. Wen, and D. L. Feng, *Phys. Rev. Lett.* **99**, 216404 (2007).
- [60] X. Wei, B. Zhao, J. Zhang, Y. Xue, Y. Li, and Z. Yang, *Phys. Rev. B* **95**, 075419 (2017).
- [61] S. Kezilebieke, M. Dvorak, T. Ojanen, and P. Liljeroth, *Nano Lett.* **18**, 2311 (2018).
- [62] Y. Zhou, Z. Wang, P. Yang, X. Zu, L. Yang, X. Sun, and F. Gao, *ACS Nano* **6**, 9727 (2012).